

Tin-accompanied and true ternary fission of ^{242}Pu

M. Zadehrafi^{1,2;1)} M. R. Pahlavani^{1,2)} M. -R. Ioan^{2;3)}

¹Department of Physics, Faculty of Basic Science, University of Mazandaran, P.O.Box 47415-416, Babolsar, Iran
²Horia Hulubei National Institute for Physics and Nuclear Engineering (IFIN-HH), P.O.Box MG-6, RO-077125, Bucharest-Magurele, Romania

Abstract: True ternary fission and Tin-accompanied ternary fission of ^{242}Pu are studied by using the 'Three Cluster Model'. True ternary fission is considered as a formation of heavy fragments in the region $28 \leq Z_1, Z_2, Z_3 \leq 38$ with comparable masses. The possible fission channels are predicted by the potential-energy calculations. Interaction potentials, Q -values and relative yields for all possible fragmentations in equatorial and collinear configurations are calculated and compared. It is found that ternary fission with formation of a double magic nucleus like ^{132}Sn is more probable than the other fragmentations. Also, the kinetic energies of the fragments for the group $Z_1 = 32, Z_2 = 32$ and $Z_3 = 30$ are calculated for all combinations in the collinear geometry as a sequential decay.

Keywords: true ternary fission, three cluster model, equatorial, collinear, kinetic energy

PACS: 24.10.-i, 25.85.-w, 25.85.Ca **DOI:** 10.1088/1674-1137/43/9/094101

1 Introduction

With the discovery of fission and its application to the production of nuclear energy in the late 1940s, most attempts of nuclear scientists had been focused logically on the study of binary fission. Ternary fission was diagnosed as an interesting source of high energy alpha particles. This rare type of nuclear reaction was discovered by the Chinese and French scientists [1–5].

Disintegration of an unstable heavy/superheavy nucleus into three fission fragments, by ignoring neutrons and other types of radiation, is termed a cold ternary fission [6–12]. Ternary fission is an appropriate tool to study the behavior of a nuclear system at the scission point of a fissioning nucleus.

True ternary fission, in which the parent nucleus breaks up into three fragments with comparable (large) masses, occurs very rarely in some heavy/superheavy nuclei with high fissility parameters [13,14]. This type of ternary fission has been studied extensively in refs. [15–25], but all of its theoretical characteristics are still not well understood.

By using the double-folding nuclear potential, a co-planar three-cluster approach was introduced into the study of the cold ternary fission of ^{252}Cf accompanied by an α particle [26]. Poenaru et al. [27–36] have developed

a macroscopic-microscopic model to study ternary fission.

According to Săndulescu et al. [37, 38], cold ternary fission can be considered like a process of cluster radioactivity; *i.e.*, a large number of nucleons are re-arranged in a cold process from the ground state of the parent to the ground state of the three final products.

Without considering the cluster preformation factors, Săndulescu et al. [39–42] have calculated the isotopic yields in the cold ternary fission of ^{248}Cm , using the double-folding potential plus M3Y nucleon-nucleon forces. Later, Florescu et al. [43] developed this model by including the preformation probability of ^4He and ^{10}Be that accompany the ternary fission of ^{252}Cf .

In the framework of the cluster picture, and as an extension of the preformed cluster model (PCM) [44], the 'Three-Cluster Model' (TCM) was introduced for studying the ternary fission process [45]. This model has been used extensively to investigate the different theoretical aspects of ternary fission for various isotopes of Cf, U, Pu and Cm [46–51].

Despite the macroscopic approach of the three-cluster model, its predictions and the obtained results are in good agreement with the available experimental data and other models [52–60].

In our first publication [61], we studied the cold ternary fission of ^{250}Cm by using the three-cluster model in

Received 19 April 2019, Published online 11 July 2019

1) E-mail: zmastaneh@theory.nipne.ro

2) E-mail: m.pahlavani@umz.ac.ir

3) E-mail: razvan.ioan@nipne.ro

©2019 Chinese Physical Society and the Institute of High Energy Physics of the Chinese Academy of Sciences and the Institute of Modern Physics of the Chinese Academy of Sciences and IOP Publishing Ltd

the equatorial geometry and considering the light charged particle as the fixed third fragment. In our second paper [62], a relatively heavy nucleus (^{34}Mg) is considered as the third fixed fragment, and is compared to the results with the light fragments in ternary fission of ^{242}Pu . The obtained results revealed that ternary fission of ^{242}Pu accompanied by ^{34}Mg occurs with very low probability in the equatorial configuration. In our recent investigation [63], the equatorial and collinear configurations in the ternary fission of ^{242}Pu accompanied by a relatively heavy ($A=14$) fragment were compared. We also compared there the results which were obtained using the proximity and Yukawa plus exponential potentials as the nuclear part of the total potential.

In the present study, we focus on the true ternary fission of ^{242}Pu in a defined region of mass and charge of the three fragments. The new aspect of this study is the variation of both the charge and mass numbers for all three fragments, which means that the area of investigation is expanded considering all possible combinations in the considered region of true ternary fission. Both equatorial and collinear geometries are considered, and the kinetic energies of the fragments for the most favorable fragmentations are calculated.

In Section 2, the theoretical framework of TCM is presented. The obtained results are presented and discussed in Section 3. Finally, a summary of the present study along with the concluding remarks is provided in Section 4.

2 Theoretical framework

In the cold ternary fission based on the three-cluster model [45], the interaction potential of the fragments is defined by

$$V = \sum_{i=1}^3 \sum_{j>i}^3 (m_x^i + V_{Cij} + V_{Nij}). \quad (1)$$

Here, m_x^i are the mass excesses of three fragments in units of energy, taken from the standard mass tables [64]. V_{Cij} and V_{Nij} are the Coulomb and nuclear potentials between each pair of the three interacting fragments, respectively. The repulsive Coulomb potential between fragments i and j , is as follows

$$\Phi(\xi) = \begin{cases} -1.7817 + 0.9270\xi + 0.0169\xi^2 - 0.05148\xi^3 & \text{for } 0 \leq \xi \leq 1.9475 \\ -4.41 \exp(-\xi/0.7176) & \text{for } \xi > 1.9475. \end{cases} \quad (9)$$

Here, $\xi = s/b$ is a function of the distance between interacting nuclei. It is assumed that in the equatorial config-

$$V_{Cij} = \frac{Z_i Z_j e^2}{C_{ij}}, \quad (2)$$

where Z_i and Z_j are the charge numbers, and C_{ij} is the distance between the centers of the two fragments i and j :

$$C_{ij} = C_i + C_j + s_{ij}. \quad (3)$$

Here, C_i and C_j are the Süssmann central radii of the nuclei, and s_{ij} is the distance between near surfaces of the nascent fragments i and j . Note that $s = 0$, $s > 0$, and $s < 0$ are related to the '*touching configuration*', '*separated geometry*', and '*overlap region*' of a pair of interacting nuclei, respectively. The Süssmann radii are taken from Ref. [65]:

$$C_x = R_x \left[1 - \left(\frac{b}{R_x} \right)^2 \right], \quad (4)$$

where the subscript x indicates the fragment number (i and $j = 1, 2$ or 3), and

$$R_x = 1.28 A_x^{1/3} - 0.76 + 0.8 A_x^{-1/3} \quad (5)$$

is the sharp radius of the fragment ' x ' with the mass number A_x . b is the diffusivity parameter of the nuclear surface (*i.e.*, $b = \frac{\pi}{\sqrt{3}}a$ with $a = 0.55$ fm) which has been evaluated to be close to unity [66]. Note that in TCM spherical shapes are considered for the decaying nucleus and all fragments [45].

In the present study, the latest version of the proximity nuclear potential (*Prox2010*) [66] is used. According to this version of the proximity potential, V_{Nij} is defined as

$$V_{Nij}(s) = V_{Pij}(s) = 4\pi b \gamma \bar{C} \Phi\left(\frac{s}{b}\right). \quad (6)$$

Here, γ is the coefficient of nuclear surface tension, which is given by

$$\gamma = 1.25284[1 - 2.345(N-Z)^2/A^2] \text{ MeV/fm}^2, \quad (7)$$

where Z , N , and A are the proton, neutron and mass numbers of the compound system, respectively. The compound system means a nuclear system composed of a pair of fission products.

\bar{C} , the mean radius of curvature, is evaluated as

$$\bar{C} = \frac{C_i C_j}{C_i + C_j}. \quad (8)$$

The universal function of the proximity potential depends on the distance between each pair of fragments. This function is defined as follows

uration, the three fission products are separated symmetrically and have the same speed. Therefore, one can as-

sume that the separation distances between each pair of fragments are equal; *i.e.*, $s = s_{12} = s_{13} = s_{23}$. In fact, the lightest fragment moves faster than the two heavier ones, due to the repulsive Coulomb force. If A_3 is the lightest fragment, the relation between the separation distances is $k \times s_{12} = s_{13} = s_{23}$, with $0 < k \leq 1$. However, it was shown in the Ref. [45] that the trends of relative yields and fragmentation potential barriers are not affected by the k -value, so consideration of $k=1$ seems a reliable assumption.

On the other hand, in the collinear configuration with A_3 in the middle, the surface distance between fragments 1 and 3 or 2 and 3 is $s = s_{13} = s_{23}$. For fragments 1 and 2, this parameter is written as

$$s_{12} = 2(C_3 + s), \quad (10)$$

where in both geometries $s = 0$ corresponds to the touching configuration. The Q -value of the cold ternary fission is given by

$$Q = M - \sum_{i=1}^3 m_i, \quad (11)$$

which should be positive to make a spontaneous reaction possible. M is the mass excess of the fissioning nucleus, and m_i is the mass excess of the fission products in units of energy. Also, since the parent and all fragments are considered in their ground state, the Q -value appears as the kinetic energy of the three fragments and can be defined as $Q = E_1 + E_2 + E_3$ with $E_i(i = 1, 2, 3)$.

The relative yield of a fragmentation channel is calculated using

$$Y(A_i, Z_i) = \frac{P(A_i, Z_i)}{\sum P(A_i, Z_i)}, \quad (12)$$

where $P(A_i, Z_i)$ is the penetrability of the i -th fragment through the three-body potential barrier. The one-dimensional WKB approximation is used to calculate the probability of penetration through the potential barrier [45],

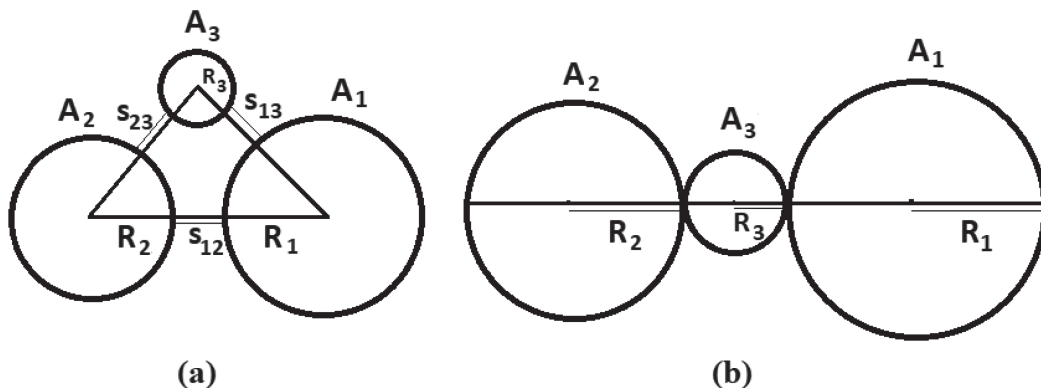


Fig. 1. A scheme of the ternary fission fragments (a) equatorial configuration for separated fragments ($s > 0$), (b) collinear touching configuration ($s = 0$).

$$P = \exp\left\{-\frac{2}{\hbar} \int_{s_1}^{s_2} \sqrt{2\mu(V-Q)} ds\right\}. \quad (13)$$

The touching configuration has been chosen as the first turning point $s_1 = 0$, and the second turning point s_2 should satisfy the equation $V(s_2) = Q$ in the above integral.

The reduced mass of the three fission products is defined as

$$\mu = m \left(\frac{A_1 A_2 A_3}{A_1 A_2 + A_1 A_3 + A_2 A_3} \right), \quad (14)$$

where m is the average mass of the nucleon, and A_1 , A_2 , and A_3 are the mass numbers of the three fragments.

A scheme of the ternary fragments in equatorial and collinear geometries is shown in Fig. 1. The touching configuration in this figure ($s = 0$), is related to the first turning point in the integral of Eq. (13).

3 Results and discussions

In the first step of the study of true ternary fission of ^{242}Pu , all possible fragmentations with $28 \leq Z \leq 38$ are extracted. The imposed condition in this research is $Z_3 \leq Z_2 \leq Z_1$, to avoid the repetition of fragment arrangements in the calculation of potential energies. Considering this condition, 14 groups of fragments with various atomic numbers are selected.

In the second step, for each group, all possible combinations with different mass numbers are listed. In each of the 14 groups, about 300 subgroups were identified. Subsequently, the interaction potentials, Q -values, penetration probabilities and relative yields were calculated for each individual fragmentation in the collinear (with the lightest fragment in the middle of the arrangement) and equatorial geometries. Note that interaction potentials are calculated in the touching-fragment configuration.

Due to the huge amount of data, presentation of all calculated results is virtually impossible. Therefore, to be

able to compare the results, the minimum of potential was chosen in each category.

The Q -values and minimum interaction potentials in the collinear and equatorial geometries are presented in Table 1. As is evident from this table, in this region of mass and charge numbers, the potential barriers of collin-

ear configurations are lower than the equatorial ones. This result has been verified with the results presented in Refs. [13, 47, 48]. Also, in most combination groups, there is at least one fragment with a neutron and/or proton closed shell (bold numbers in Table 1).

Table 1. Q -values and minimum interaction potentials for 14 groups of Z_1 , Z_2 and Z_3 between 28 and 38, with the condition $Z_3 \leq Z_2 \leq Z_1$. Seven highlighted groups are shown in Fig. 9 for visual comparison.

Z_1	Z_2	Z_3	Z_1	Z_2	Z_3	Z_1	Z_2	Z_3	Q/MeV	$V_{\text{tot}} - \text{collinear}/\text{MeV}$	$V_{\text{tot}} - \text{equatorial}/\text{MeV}$
32	31	31	82	79	81	50	48	50	240.3094	78.1659	100.605
32	32	30	82	82	78	50	50	48	243.032	74.4898	97.7208
33	31	30	83	81	78	50	50	48	239.4991	77.9527	101.1142
33	32	29	83	82	77	50	50	48	238.313	77.4297	101.9928
33	33	28	83	83	76	50	50	48	235.6672	78.0857	103.7011
34	30	30	84	78	80	50	48	50	239.7981	76.8431	99.9926
34	31	29	84	81	77	50	50	48	236.8043	78.8	102.739
34	32	28	86	82	74	52	50	46	239.0969	75.2326	100.4867
35	30	29	87	78	77	52	48	48	234.6038	80.6331	104.5678
35	31	28	87	81	74	52	50	46	234.6986	79.3986	104.4263
36	29	29	90	75	77	54	46	48	232.6591	82.0497	105.9731
36	30	28	90	78	74	54	48	46	235.621	78.0305	102.8422
37	29	28	93	75	74	56	46	46	230.2699	82.7749	107.2704
38	28	28	94	74	74	56	46	46	230.4843	81.81	105.7355

In the group $Z_1 = 32$, $Z_2 = 32$, and $Z_3 = 30$, which has the lowest minimum interaction potential among all 14 groups, the most favorable combinations with the same A_1 are chosen and the variations of the interacting potentials, Q -values and relative yields are plotted as a function of the fragment mass number A_1 . The results are presented in Fig. 2. Note that the three vertical axes in this figure have a different scale.

From Fig. 2, it is obvious that an increase of the Q -value and relative yield is equivalent to a decrease of the interaction potential, and vice versa. However, this equivalence is not always valid. In Fig. 2, the Z values are constant in all considered combinations. If both Z and A vary among different combinations, one may see that there is no specific relation between the Q -values and relative yields or interaction potentials (see subsection 3.1).

In Fig. 2, the minimum of the interaction potential and the maximum of the yields and Q -values occurs for the combination $^{82}\text{Ge} + ^{78}\text{Zn} + ^{82}\text{Ge}$ with the magic neutron number for the two Ge isotopes ($N = 50$). For this group ($Z_1 = 32$, $Z_2 = 32$, and $Z_3 = 30$), the contour map is generated considering all 300 possible combinations with various mass numbers. It can be seen that the maxima of

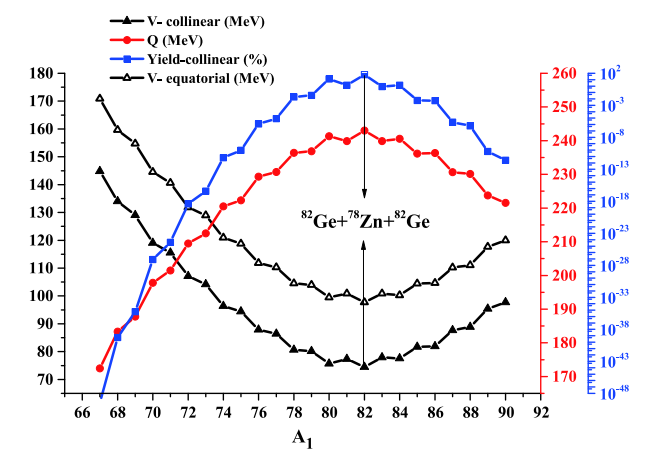


Fig. 2. (color online) Interaction potentials in the collinear and equatorial configurations (left vertical axis), Q -values (right vertical axis), and relative yields in the collinear geometry (logarithmic axis) for the combinations with $Z_1 = 32$, $Z_2 = 32$, $Z_3 = 30$ and different mass numbers, plotted as a function of A_1 .

the Q -values (Fig. 3), which correspond to the minima of the interaction potentials (Fig. 4), belong to a region where the mass numbers A_1 and A_2 (and consequently A_3)

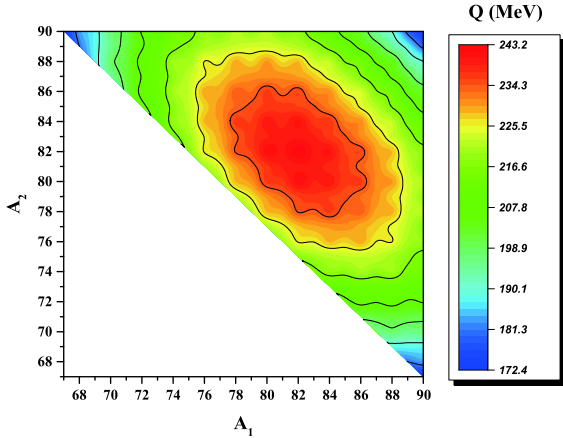


Fig. 3. (color online) Contour map of the Q -values for all possible combinations of the breakup $^{242}\text{Pu} \rightarrow A_1 \text{Ge} + A_3 \text{Zn} + A_2 \text{Ge}$, plotted as a function of fragment mass numbers A_1 and A_2 .

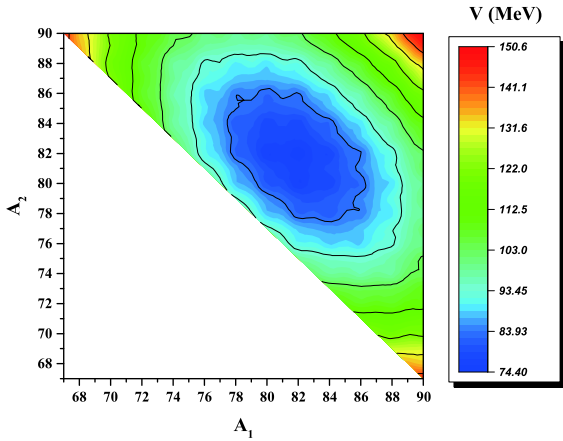


Fig. 4. (color online) Contour map of the interaction potentials (collinear geometry) for all possible combinations of the breakup $^{242}\text{Pu} \rightarrow A_1 \text{Ge} + A_3 \text{Zn} + A_2 \text{Ge}$, plotted as a function of fragment mass numbers A_1 and A_2 .

are close together. This region can be considered as the region of true ternary fission.

From an analysis of Table 1 one can conclude that: (1) even-mass fragments have lower potential barriers than the odd-mass ones (in agreement with [46, 47, 67, 68]); (2) neutron closed shell structures are more important than the proton closed shells for lowering the potential barrier (compatible with [45, 69]); (3) the closed shell structure of the heaviest fragment plays a key role for the more favorable channels (in agreement with [69]); (4) fragments with smaller difference of mass numbers have lower potential barriers and higher Q -values compared to other fragmentations (upper and lower rows of Table 1).

3.1 Comparison between true and Tin-accompanied ternary fission of ^{242}Pu

In this part of the study, we consider a double magic

nucleus (^{132}Sn) as the fixed fragment and compare it with the previous results for true ternary fission of ^{242}Pu . Like in the previous section, all possible ternary channels are considered. The Q -values and charge minimized potentials in the equatorial and collinear configurations were calculated and are plotted as a function of A_3 (the lightest fragment) in Figs. 5 and 6, respectively. As is clear from these figures, there is no specific relation between the Q -values and the interaction potentials, due to the variation of both A and Z . In fact, the actual possibility of ternary fission is related to the potential barrier properties and not to the released energy.

It can be seen in Fig. 6 that collinear geometry has a lower potential barrier than the equatorial geometry, except for very light third fragment. The lowest barrier in collinear geometry is obtained for the combination $^{132}\text{Sn} + ^{22}\text{O} + ^{88}\text{Kr}$. A similar results for ternary fission of ^{252}Cf were reported in Ref. [53].

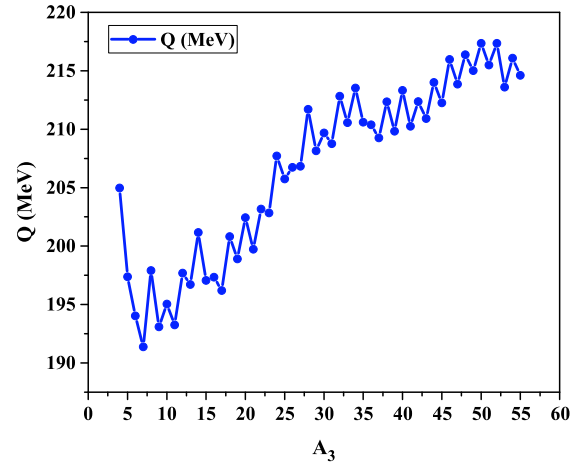


Fig. 5. (color online) Q -values for the breakup $^{242}\text{Pu} \rightarrow ^{132}\text{Sn} + A_3 + A_2$.

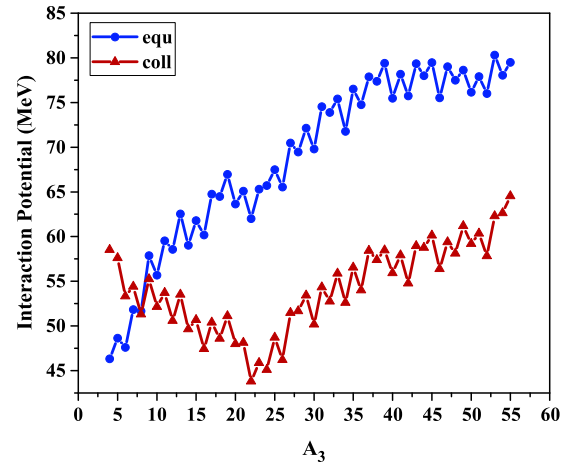


Fig. 6. (color online) Charge minimized interaction potentials for the breakup $^{242}\text{Pu} \rightarrow ^{132}\text{Sn} + A_3 + A_2$ in the collinear and equatorial geometries.

Variation of the potential barrier ($V_C + V_P$) as a function of separation parameter (s) is presented in Fig. 7 for the combination $^{132}\text{Sn} + ^{22}\text{O} + ^{88}\text{Kr}$. The potential is calculated by varying s uniformly, starting from the touching configuration ($s_1 = 0$) to the point s_0 ($V(s_0) = Q$). It should be mentioned here that the potentials in the overlap region are not favored in this model. Indeed, shifting the first turning point from the touching configuration ($s_1 = 0$) to the point s_0 ($V(s_0) = Q$) leads to the model of Shi and Swiatecki (Ref. [70]) for penetrability calculations. More information about the calculation of penetrability by using the two turning points is given in Refs. [44, 45, 61, 62].

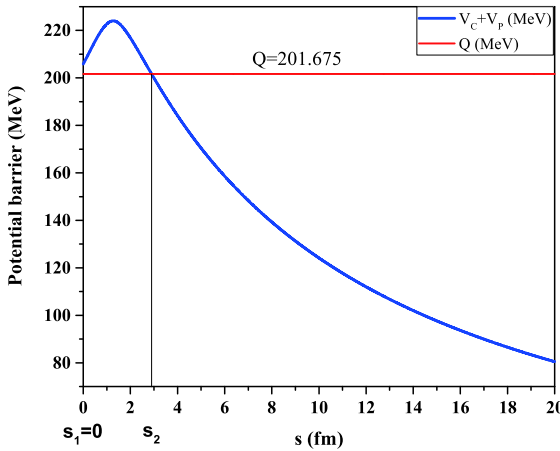


Fig. 7. (color online) Potential barrier ($V_C + V_P$) as a function of separation parameter s for the breakup $^{242}\text{Pu} \rightarrow ^{132}\text{Sn} + ^{22}\text{O} + ^{88}\text{Kr}$. The turning points and the Q -value are also shown.

In Fig. 8, the interaction potentials in the region of true ternary fission ($Z_1 = 32, Z_2 = 32, Z_3 = 30$) and Tin-accompanied ternary fission of ^{242}Pu are compared. It is obvious from this figure that in collinear configuration the

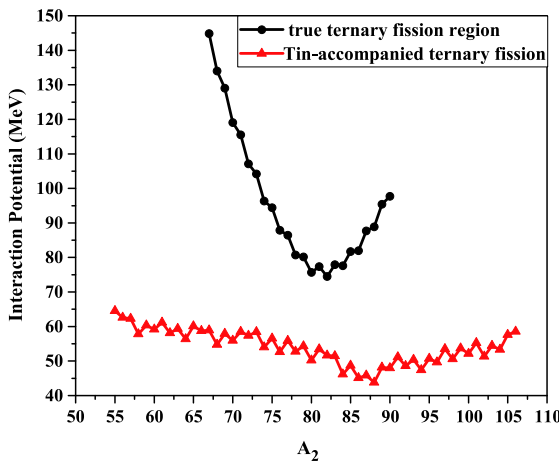


Fig. 8. (color online) Comparison of the potential barriers for true ternary fission and Tin-accompanied ternary fission of ^{242}Pu in the collinear configuration.

ternary potential barriers with ^{132}Sn as the fixed fragment are much lower than for the other groups. Since ^{132}Sn is a double magic isotope ($Z = 50$ and $N = 82$), this result emphasizes the importance of the closed shell structures for the favorable ternary channels.

In order to get a better visual comparison, seven groups with different Z_1 (highlighted in Table 1) are shown in Fig. 9 as a bar graph. The combination $^{132}\text{Sn} + ^{22}\text{O} + ^{88}\text{Kr}$ is also shown in this figure. It is evident that in these seven groups there is no significant difference between the magnitudes of interaction potentials for fragments with various Z (less than 10 MeV). But the ternary fragmentation potential barrier with ^{132}Sn as the fixed fragment is almost 30 MeV lower than the others.

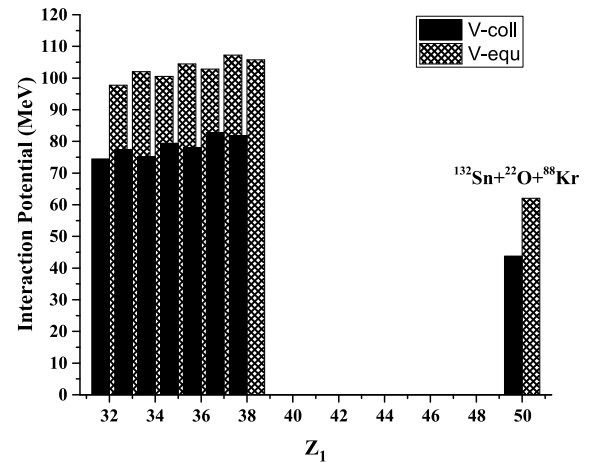


Fig. 9. Comparison of the minimum interaction potentials for true and Tin-accompanied ternary fission of ^{242}Pu in the collinear and equatorial geometries.

3.2 Kinetic energy of the fragments in the group $Z_1 = 32, Z_2 = 32$, and $Z_3 = 30$

In order to calculate the kinetic energies of the fragments, we concentrate on the fragmentation $^{242}\text{Pu} \rightarrow ^{A_1}\text{Ge} + ^{A_2}\text{Zn} + ^{A_3}\text{Ge}$, which has the lowest potential barrier among the 14 groups. Also, the collinear tripartition is considered as a sequential decay, which means that the ternary fragmentation happens in two steps. In the first step, the unstable parent nucleus with mass number A breaks into fragments A_i and A_{jk} . Then in the next step, the composite fragment A_{jk} fissions into fragments A_j and A_k . In this study, i, j and k are referred to fragment numbers 1, 3, and 2, respectively. We assume that in both steps the energy and momentum of the system are conserved. In order to calculate the kinetic energy, we employ the method presented in Ref. [49]. The mathematical method for calculating the kinetic energy is presented here briefly. For more details, the interested reader can consult Ref. [49].

$$Q_I = M_x(A) - [m_x(A_1) + m_x(A_{23})]. \quad (15)$$

$$Q_{II} = m_x(A_{23}) - [m_x(A_2) + m_x(A_3)]. \quad (16)$$

Equations (15) and (16) are related to the steps one and two, respectively. M_x is the mass excess of the parent, and m_x is the mass excess of the fragments in each step.

In the first step, the velocity of the composite nucleus is obtained using

$$v_{23} = + \sqrt{\left(\frac{2m_1}{m_1 + m_{23}}\right)\left(\frac{Q_I}{m_{23}}\right)}, \quad (17)$$

and similarly, the velocity of fragment 1 is as follows

$$v_1 = - \sqrt{\left(\frac{2m_{23}}{m_1 + m_{23}}\right)\left(\frac{Q_I}{m_1}\right)}. \quad (18)$$

Here, m is the mass of the fragments expressed in units of energy.

For the velocities of fragments 2 and 3 in the second step, we have

$$v_2 = \frac{m_2 m_{23} v_{23} \pm \sqrt{\zeta^2}}{m_2^2 + m_2 m_3}, \quad (19)$$

where

$$\begin{aligned} \zeta^2 = & m_2^2 m_{23}^2 v_{23}^2 - [(m_2^2 + m_2 m_3) \\ & \times (m_{23}^2 v_{23}^2 - 2m_3 Q_{II} - m_3 m_{23} v_{23}^2)]. \end{aligned} \quad (20)$$

$$v_3 = - \left[\frac{m_2 v_2 - m_{23} v_{23}}{m_3} \right]. \quad (21)$$

Finally, using the well known formula $E = \frac{1}{2}mv^2$, the kinetic energies of all three fragments are obtained.

The kinetic energies of the fragments A_1 Ge and A_3 Zn are shown in Figs. 10 and 11 as a function of A_1 and A_2 for all 300 combinations.

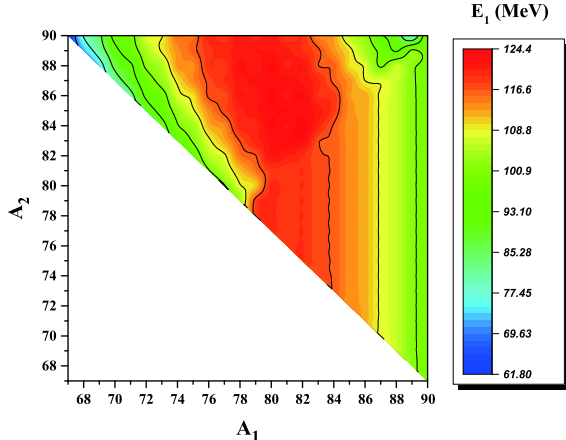


Fig. 10. (color online) Kinetic energy of the fragment A_1 Ge as a function of A_1 and A_2 for the collinear breakup $^{242}\text{Pu} \rightarrow A_1 \text{ Ge} + A_3 \text{ Zn} + A_2 \text{ Ge}$.

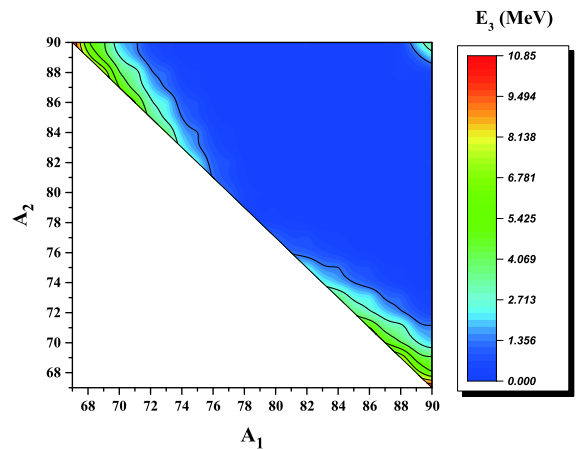


Fig. 11. (color online) Kinetic energy of the fragment A_3 Zn as a function of A_1 and A_2 for the collinear breakup $^{242}\text{Pu} \rightarrow A_1 \text{ Ge} + A_3 \text{ Zn} + A_2 \text{ Ge}$.

As is clear from Fig. 11, the light fragment that is located in the middle of the collinear arrangement takes a very small part of the total kinetic energy, and the major part of the total kinetic energy is removed by the other two fragments. This observation could be the reason why the light fragment has escaped experimental detection. This result is in agreement with Ref. [49].

The kinetic energies of the fragments for the combinations mentioned in Fig. 2 are presented as a two dimensional graph in Fig. 12. The relative yields, Q -values and total kinetic energies of this group are also listed in Table 2. One may observe that the Q -values and total kinetic energies for each fragmentation in Table 2 are almost equal. This result is due to the assumption that ternary fission is a cold process.

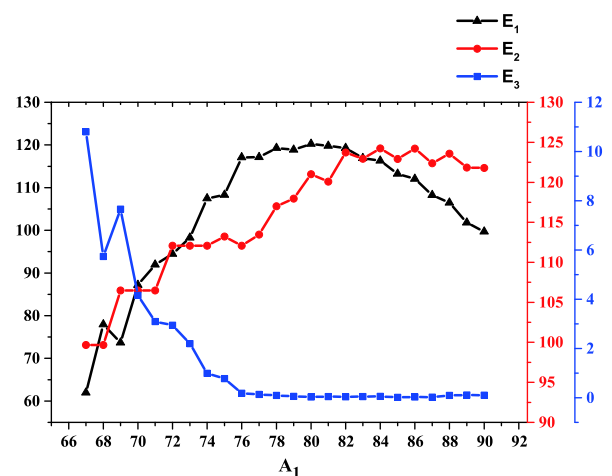


Fig. 12. (color online) Kinetic energies of the fragments A_1 , A_2 and A_3 for the sequential collinear decay $^{242}\text{Pu} \rightarrow A_1 \text{ Ge} + A_3 \text{ Zn} + A_2 \text{ Ge}$. Vertical axes are (from left to right) for E_1 , E_2 , and E_3 . It is clear that the fragment number 3 is almost at rest.

Table 2. Calculated data for the breakup $^{242}\text{Pu} \rightarrow ^{A_1}\text{Ge} + ^{A_3}\text{Zn} + ^{A_2}\text{Ge}$. For each value of A_1 , the interaction potential is minimized. Therefore, 24 combinations among 300 are chosen (yields less than 10^{-7} are denoted as "0").

A_1	A_2	A_3	relative yield – collinear (%)	relative yield – equatorial (%)	Q /MeV	total kinetic energy /MeV
67	90	85	0.000	0.000	172.437	172.438
68	90	84	0.000	0.000	183.327	183.329
69	88	85	0.000	0.000	187.799	187.801
70	88	84	0.000	0.000	197.830	197.832
71	88	83	0.000	0.000	201.505	201.506
72	86	84	0.000	0.000	209.474	209.476
73	86	83	0.000	0.000	212.516	212.517
74	86	82	0.000	0.000	220.511	220.512
75	85	82	0.000	0.000	222.309	222.310
76	86	80	1.26×10^{-6}	0.000	229.340	229.341
77	85	80	8.34×10^{-6}	0.000	230.703	230.704
78	84	80	1.98×10^{-2}	1.25×10^{-3}	236.377	236.379
79	83	80	3.66×10^{-2}	2.78×10^{-3}	236.874	236.875
80	82	80	13.00	5.23	241.318	241.319
81	82	79	1.39	0.457	239.858	239.859
82	82	78	61.7	92.1	243.032	243.033
83	82	77	0.817	0.512	239.899	239.901
84	82	76	1.38	1.68	240.585	240.586
85	80	77	5.79×10^{-3}	8.85×10^{-4}	236.166	236.167
86	80	76	5.17×10^{-3}	1.25×10^{-3}	236.317	236.318
87	79	76	2.28×10^{-6}	0.000	230.632	230.633
88	80	74	6.11×10^{-7}	0.000	230.151	230.152
89	79	74	0.000	0.000	223.735	223.737
90	78	74	0.000	0.000	221.557	221.559

4 Conclusion

True ternary fission of ^{242}Pu was studied and compared with the Tin-accompanied ternary fission of the parent. The most probable ternary fission path is predicted to be the one with the minimum interaction potential with respect to the mass and charge asymmetries. The obtained results revealed that in the considered region of mass and charge numbers ($28 \leq Z_1, Z_2, Z_3 \leq 38$), the collinear geometry is preferred to the equatorial geometry. Also, closed shell structures play an inevitable role in the potential barrier height. Indeed, closed neutron shells are more effective in lowering the potential barrier than the closed proton shells. The most favorable combinations are in a region where the fragments have comparable

mass and charge numbers.

However, it is found that the Tin-accompanied ternary fission of ^{242}Pu is more favorable than the true ternary fission. This can be interpreted in two ways: (1) ^{132}Sn is a magic nucleus, both in proton and neutron numbers; (2) three fragments with comparable sizes (true ternary fission) are less likely to appear in the exit channel.

The kinetic energies of the fragments in the group $Z_1 = 32$, $Z_2 = 32$, and $Z_3 = 30$ were also calculated in the collinear geometry as a sequential decay. The obtained results showed that a large fraction of the total kinetic energy is carried by the two Ge nuclei, and Zn, as the middle part of the arrangement, does not have significant kinetic energy. This fact can be the reason why it has escaped experimental detection.

References

- 1 San-Tsiang, Chastel, Zah-Wei et al, Comptes Rendus, **223**: 986 (1946)
- 2 San-Tsiang, Zah-Wei, Chastel et al, Comptes Rendus, **224**: 272 (1947)
- 3 San-Tsiang, Zah-Wei, Chastel et al, Phys. Rev., **71**: 382 (1947)
- 4 T. San-Tsiang, H. Zah-Wei, R. Chaste et al, *J. Phys. Radium*, **8**: 165 (1947)
- 5 T. San-Tsiang, H. Zah-Wei, L. Vigneron et al, *Nature*, **159**: 773 (1947)
- 6 L. W. Alvarez, G. Farwell, E. Segrè et al, *Phys. Rev.*, **71**: 327 (1947)
- 7 L. Rosen and A.M. Hudson, *Phys. Rev.*, **78**: 533 (1950)
- 8 P. Fong, *Phys. Rev. C*, **2**: 735 (1970)
- 9 P. B. Vitta, *Nucl. Phys. A*, **170**: 417 (1971)
- 10 C. Wagemans and A.J. Deruyter, *Nucl. Phys. A*, **194**: 657 (1972)
- 11 J. P. Théobald, P. Heeg, and M. Mutterer, *Nucl. Phys. A*, **502**: 343 (1989)
- 12 G. Royer, F. Haddad, and J. Mignen, *J. Phys. G: Nucl. Part. Phys.*, **18**: 2015 (1992)
- 13 K. R. Vijayaraghavan and M. Balasubramaniam, *Phys. Rev. C*, **91**: 044616 (2015)
- 14 W. von Oertzen and A. K. Nasirov, *Phys. Lett. B*, **734**: 234 (2014)
- 15 J. C. Roy, *Canad. J. Phys.*, **39**: 315 (1961)
- 16 R. W. Stoenner and M. Hillman, *Phys. Rev.*, **142**: 716 (1966)
- 17 M. L. Muga, C. R. Rice, and W. A. Sedlacek, *Phys. Rev.*, **161**: 1266 (1967)
- 18 K. W. MacMurdo and J. W. Cobble, *Phys. Rev.*, **182**: 1303 (1969)
- 19 G. Kugler and W. B. Clarke, *Phys. Rev. C*, **3**: 849 (1971)
- 20 P. A. Gottschalk et al, *Phys. Rev. Lett.*, **42**: 359 (1979)
- 21 P. A. Gottschalk, G. Grawert, P. Vater et al, *Phys. Rev. C*, **27**: 2703 (1983)
- 22 H.-Y. Wu et al, *Phys. Rev. C*, **57**: 3178 (1998)
- 23 C.-M. Herbach et al, *Nucl. Phys. A*, **712**: 207 (2002)
- 24 Yu. V. Pyatkov et al, *Phys. At. Nucl.*, **67**: 1726 (2004)
- 25 Yu. V. Pyatkov et al, *Eur. Phys. J. A*, **45**: 29 (2010)
- 26 A. Săndulescu, F. Carstoiu, I. Bulboaca et al, *Phys. Rev. C*, **60**: 044613 (1999)
- 27 D. N. Poenaru et al, *J. Phys. G: Nucl. Part. Phys.*, **26**: L97 (2000)
- 28 D. N. Poenaru et al, Rom. Rep. Phys., **55**: 549 (2003)
- 29 D. N. Poenaru, R. A. Gherghescu, and W. Greiner, *Nucl. Phys. A*, **747**: 182 (2005)
- 30 R. A. Gherghescu, D. N. Poenaru, and W. Greiner, *J. Phys. G: Nucl. Part. Phys.*, **23**: 1715 (1997)
- 31 D. N. Poenaru, W. Greiner, J. H. Hamilton, and A. V. Ramayya, APH N. S., *Heavy Ion Physics*, **14**: 285 (2001)
- 32 R. A. Gherghescu, D. N. Poenaru, and W. Greiner, Rom. J. Phys., **50**: 377 (2005)
- 33 D. N. Poenaru, R. A. Gherghescu, and W. Greiner, *Phys. Rev. Lett.*, **107**: 062503 (2011)
- 34 D. N. Poenaru, R. A. Gherghescu, and W. Greiner, *Phys. Rev. C*, **85**: 034615 (2012)
- 35 D. N. Poenaru, R. A. Gherghescu, and W. Greiner, *J. Phys. G: Nucl. Part. Phys.*, **40**: 105105 (2013)
- 36 R. A. Gherghescu and D. N. Poenaru, *Pramana J. Phys.*, **85**: 439 (2015)
- 37 A. Săndulescu et al, *Phys. Rev. C*, **57**: 2321 (1998)
- 38 D. S. Delion, A. Florescu, and A. Săndulescu, *Phys. Rev. C*, **63**: 044312 (2001)
- 39 A. Săndulescu et al, *J. Phys. G: Nucl. Part. Phys.*, **24**: 181 (1998)
- 40 A. Săndulescu et al, *Int. J. Mod. Phys. E*, **7**: 625 (1998)
- 41 A. Săndulescu et al, *J. Phys. G: Nucl. Part. Phys.*, **23**: L7 (1997)
- 42 A. Săndulescu et al, *Phys. Rev. C*, **54**: 258 (1996)
- 43 A. Florescu et al, *Phys. Rev. C*, **61**: 051602 (2000)
- 44 S. S. Malik and R. K. Gupta, *Phys. Rev. C*, **39**: 1992 (1989)
- 45 K. Manimaran and M. Balasubramaniam, *Phys. Rev. C*, **79**: 024610 (2009)
- 46 K. Manimaran and M. Balasubramaniam, *Eur. Phys. J. A*, **45**: 293 (2010)
- 47 K. Manimaran and M. Balasubramaniam, *Phys. Rev. C*, **83**: 034609 (2011)
- 48 K. R. Vijayaraghavan, M. Balasubramaniam, and W. von Oertzen, *Phys. Rev. C*, **90**: 024601 (2014)
- 49 K. R. Vijayaraghavan, W. von Oertzen, and M. Balasubramaniam, *Eur. Phys. J. A*, **48**: 27 (2012)
- 50 K. Manimaran and M. Balasubramaniam, *J. Phys. G: Nucl. Part. Phys.*, **37**: 045104 (2010)
- 51 M. Balasubramaniam, K. R. Vijayaraghavan, and K. Manimaran, *Phys. Rev. C*, **93**: 014601 (2016)
- 52 V. I. Zagrebaev, A. V. Karpov, and W. Greiner, *Phys. Rev. C*, **81**: 044608 (2010)
- 53 V. Yu. Denisov, N. A. Pilipenko, and I. Yu. Sedykh, *Phys. Rev. C*, **95**: 014605 (2017)
- 54 A. V. Karpov, *Phys. Rev. C*, **94**: 064615 (2016)
- 55 W. von Oertzen, A. K. Nasirov, and R. B. Tashkhodjaev, *Phys. Lett. B*, **746**: 223 (2015)
- 56 G. G. Adamian et al, *Int. J. Mod. Phys. E*, **17**: 2014 (2008)
- 57 A. V. Andreev et al, *Eur. Phys. J. A*, **30**: 579 (2006)
- 58 A. K. Nasirov, R. B. Tashkhodjaev, and W. von Oertzen, *Eur. Phys. J. A*, **52**: 135 (2016)
- 59 R. B. Tashkhodjaev et al, *Phys. Rev. C*, **91**: 054612 (2015)
- 60 R. B. Tashkhodjaev, A. K. Nasirov, and E. Kh. Alpomeshev, *Phys. Rev. C*, **94**: 054614 (2016)
- 61 M. R. Pahlavani, O. N. Ghodsi, and M. Zadehrafi, *Phys. Rev. C*, **96**: 054612 (2017)
- 62 M. R. Pahlavani and M. Zadehrafi, *Eur. Phys. J. A*, **54**: 128 (2018)
- 63 M. Zadehrafi et al, Rom. J. Phys., **64**: 304 (2019)
- 64 M. Wang et al, *Chin. Phys. C*, **41**: 030003 (2017)
- 65 J. Blocki, J. Randrup, W. J. Swiatecki et al, *Ann. Phys. (N.Y.)*, **105**: 427 (1977)
- 66 I. Dutt and R. Bansal, *Chin. Phys. Lett.*, **27**: 112402 (2010)
- 67 K. P. Santhosh, S. Krishnan, and B. Priyanka, *Eur. Phys. J. A*, **50**: 66 (2014)
- 68 K. P. Santhosh, S. Krishnan, and B. Priyanka, *Int. J. Mod. Phys. E*, **23**: 1450071 (2014)
- 69 M. Ismail, W. M. Seif, A. Y. Ellithi et al, *Can. J. Phys.*, **91**: 401 (2013)
- 70 Y. J. Shi and W. Swiatecki, *Phys. Rev. Lett.*, **54**: 300 (1985)